

# Electronic Structure



## OPEN ACCESS

RECEIVED  
21 December 2023

REVISED  
30 May 2024

ACCEPTED FOR PUBLICATION  
17 June 2024

PUBLISHED  
27 June 2024

Original Content from  
this work may be used  
under the terms of the  
[Creative Commons  
Attribution 4.0 licence](#).

Any further distribution  
of this work must  
maintain attribution to  
the author(s) and the title  
of the work, journal  
citation and DOI.



## PAPER

# Effect of molecular rotation and concentration on the adsorption of pentacene molecules on two-dimensional monolayer transition metal dichalcogenides

E Black\* and J M Morbec

School of Chemical and Physical Sciences, Keele University, Keele ST5 5BG, United Kingdom

\* Author to whom any correspondence should be addressed.

E-mail: [e.j.black@keele.ac.uk](mailto:e.j.black@keele.ac.uk)

**Keywords:** 2D materials, vdW heterostructures, photovoltaics, organic/2D heterostructures

Supplementary material for this article is available [online](#)

## Abstract

Heterostructures composed of pentacene (PEN) molecules and transition metal dichalcogenides (TMDs) are promising materials for small, flexible and lightweight photovoltaic devices and various other optoelectronic applications. The effects of changing concentration and orientation of adsorbed PEN molecules on two-dimensional monolayer substrates of TMDs, namely MoS<sub>2</sub>, MoSe<sub>2</sub>, WS<sub>2</sub> and WSe<sub>2</sub>, were investigated using first-principles calculations based on density functional theory. We examined the structural and electronic properties of the corresponding PEN/TMD heterostructures and compared these between differing PEN concentrations and the orientations of PEN with respect to the underlying substrate crystal structure. We analyze the band alignment of the heterostructures and demonstrate a concentration-dependent staggered-to-straddling (typeII-I) band gap transition in PEN/MoSe<sub>2</sub>.

## 1. Introduction

Two-dimensional monolayers of transition metal dichalcogenides (TMDs), namely MoS<sub>2</sub>, MoSe<sub>2</sub>, WS<sub>2</sub> and WSe<sub>2</sub>, readily form van der Waals (vdW) heterostructures with other lattices or molecules [1]. The weak vdW interactions allow for easy combinations of heterogeneous materials, potentially giving rise to novel properties [2, 3]. Monolayer TMDs exhibit favorable optical absorption properties [4–6] with many applications, such as photovoltaics [7], field-effect transistors [8, 9] and LED technologies [10], all while being thin and flexible enough for wearable, lightweight devices [11]. Additionally, TMD crystals exfoliate to few-layer systems with no dangling bonds, permitting the formation of vdW heterostructures [2]. Creating these vdW heterostructures from TMDs and another semiconducting compound with complimentary electronic properties and band alignment may be a way to improve potential for use in a variety of technological applications, including photovoltaic devices, electrochemical biosensors and chemical catalysts [12].

Organic compounds are a large family of structures with diverse properties and are often readily synthesized, where the adsorption of organic molecules to TMDs has been shown to modulate their electronic properties [13], in addition to potentially having complimentary properties to the TMD for a given application. One such organic molecule is pentacene (PEN) (C<sub>22</sub>H<sub>14</sub>). A popular material for combination with TMDs, PEN boasts strong visible-range spectral absorption [14], high carrier mobility and photosensitivity [15, 16], and as shown in previous works [17], exhibits type-II band alignment when in interface with MoS<sub>2</sub>, MoSe<sub>2</sub>, and WS<sub>2</sub>. PEN/MoS<sub>2</sub> heterostructures have been shown to exhibit rapid exciton dissociation with recombination lifetimes an order of magnitude longer than those in TMD/TMD heterostructures [18]. Existing literature focuses on thin films of adsorbed PEN rather than truly 2D structures [19, 20], and is mostly limited to adsorption on MoS<sub>2</sub>. The growth mechanism of PEN films is a crucial area of study, where growth on Ag(111) and Au(111) have been investigated for the structures' use in

thin film transistors [21], as well as on copper and iron substrates [22, 23]. Limited theoretical literature exists for the determination of the most favorable adsorption site of PEN on TMDs across molecular concentrations, the effect of molecular rotation and the resultant strength of molecule–substrate coupling and electronic interaction. Understanding the manner in which PEN will tend to adsorb on a TMD substrate is important for device design and tuning, as it can affect device performance through changes in electronic structure and device-specific interface engineering concerns.

Here systems of PEN adsorbed upon  $\text{MoS}_2$ ,  $\text{MoSe}_2$ ,  $\text{WS}_2$  and  $\text{WSe}_2$  are investigated, examining the effect of adsorbate concentration and flat-lying rotation with respect to the underlying substrate. Adsorbate concentration was controlled by using one PEN molecule in two different sizes of supercell; a  $6 \times 3$  supercell, which corresponds to molecular concentrations of one PEN molecule per  $157 \text{ \AA}^2$  (sulphide systems),  $170 \text{ \AA}^2$  ( $\text{MoSe}_2$ ), or  $169 \text{ \AA}^2$  ( $\text{WSe}_2$ ), and a  $7 \times 4$  supercell, which corresponds to molecular concentrations of one PEN per  $244 \text{ \AA}^2$  (sulphide systems),  $264 \text{ \AA}^2$  ( $\text{MoSe}_2$ ), or  $263 \text{ \AA}^2$  ( $\text{WSe}_2$ ).

## 2. Computational details

*Ab initio* calculations based on density functional theory (DFT) [24] were performed on PEN/TMD heterostructures, with the initial structural parameters and position of the center of mass of PEN with respect to the underlying substrate determined via geometric optimization. PEN adsorption sites investigated are top-transition metal (top-TM), top-Chalcogen (top-Ch), bridge-A, bridge-B and hollow (figure 1).

The calculations were performed using the Quantum Espresso suite [25, 26] using the plane wave pseudopotential method within DFT. The Perdew–Burke–Ernzenhof (PBE) exchange–correlation potential approximation [27], a generalized gradient approximation (GGA), was used alongside Grimme’s DFT-D3 vdW force corrections [28]. Projector-augmented wave (PAW) [29] pseudopotentials were used. A vertical vacuum region of approximately  $45 \text{ \AA}$  maintains repeated images of the heterostructure isolated from each other in the supercell approach with periodic boundary conditions. For geometric optimization, an energy convergence of  $10^{-4} \text{ Ry}$  was achieved using wavefunction cutoffs of 80, 100, 80 and 120 Ry for  $\text{MoS}_2$ ,  $\text{MoSe}_2$ ,  $\text{WS}_2$  and  $\text{WSe}_2$  respectively (determined after convergence tests). Kinetic energy cut-offs were similarly 320, 400, 320 and 480 Ry, and a Monkhorst–Pack [30] k-point mesh of  $3 \times 6 \times 1$  was employed. The k-point convergence testing was carried out for both concentration regimes independently. Self-consistent field calculations were performed with the optimized geometry, using the same k-point meshes as in the relaxation calculations. Non-self-consistent field calculations followed, using denser k-point meshes of  $6 \times 12 \times 1$ . Density of states (DOS) and projected density of states (pDOS) calculations were then performed for the most favorable structures. These calculations were performed with the Gaussian smearing method for Brillouin Zone integration, a simple Gaussian broadening of 0.005 eV and energy grid step of 0.05 eV. A summary of computational details can be found in table S1 of the supplementary material.

## 3. Results

In this work we investigate both the effects of molecular concentration and rotation on the electronic properties of PEN/TMD heterostructures. We first focused on the molecular concentration, discussed in the first subsection of Results (section 3.1). The effect of rotation is discussed in the following subsection (section 3.2).

### 3.1. Effect of molecular concentration

Investigated here is the high concentration regime of PEN, where we considered a single PEN molecule adsorbed on a  $6 \times 3$  supercell of the TMD substrate. The long axis of the PEN is aligned with the long axis of the underlying substrate crystal ( $0^\circ$  of rotation). The supercells (without PEN) are represented in figure S2 of the supplementary material.

In the  $6 \times 3$  systems minimum molecule–molecule separation on periodic boundary conditions is found to be approximately  $3.4 \text{ \AA}$  for sulphide systems, and  $3.7 \text{ \AA}$  for selenide systems, which have lattice parameters of  $3.17 \text{ \AA}$  for both  $\text{MoS}_2$  and  $\text{WS}_2$ , and  $3.30 \text{ \AA}$  and  $3.29 \text{ \AA}$  for  $\text{MoSe}_2$  and  $\text{WSe}_2$ , respectively [17]. The same five absorption sites investigated in [17] have been revisited here in a higher PEN concentration regime. These are displayed in figure 1 and defined by where on the substrate lattice the central PEN ring lies over. The central ring of PEN lies over a bond between a transition metal atom (Mo or W) and a chalcogen atom (S or Se) in the bridge-A and bridge-B sites (figures 1(a) and (b), respectively), over the empty space between within the crystal structure’s hexagon in the hollow site (figure 1(c)), on top of a transition metal atom (Mo or W) in the top-TM site (figure 1(d)), or over a chalcogen atom (S or Se) in the top-Ch site (figure 1(e)).

Following geometric optimization, top-TM is found to be the most favorable binding site for  $\text{MoS}_2$ ,  $\text{MoSe}_2$  finds bridge-B to be most favorable,  $\text{WS}_2$  finds top-Ch to be most favorable, and  $\text{WSe}_2$  finds bridge-A

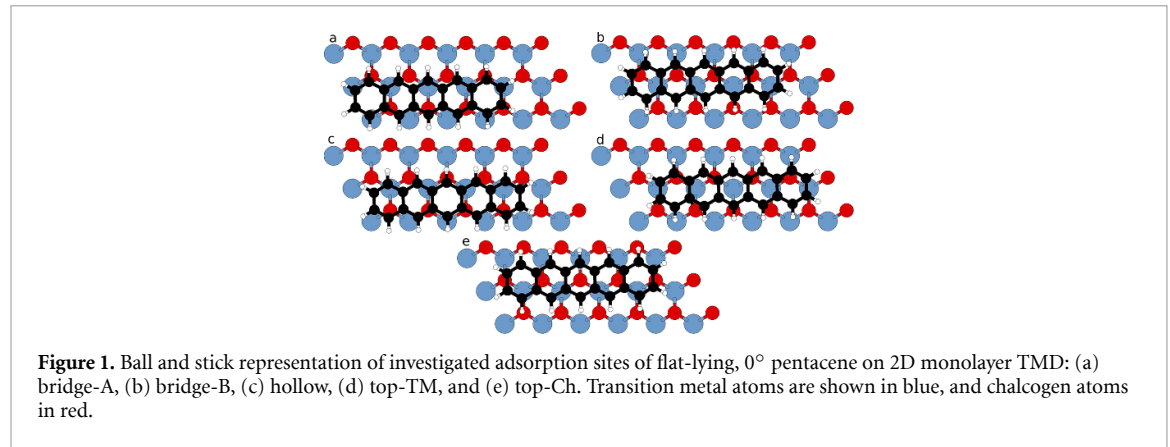


**Table 1.** Adsorption energies, in eV, following geometry optimization of the  $6 \times 3$  PEN/TMD heterostructures. Most favorable binding sites are highlighted in bold, and binding site geometries are displayed in figure 1.

TMD	Bridge-A	Bridge-B	Hollow	Top-TM	Top-Ch
MoS <sub>2</sub>	−1.318	−1.413	−1.363	<b>−1.461<sup>a</sup></b>	−1.407
MoSe <sub>2</sub>	−1.348	<b>−1.437</b>	−1.387	−1.377	−1.432
WS <sub>2</sub>	−1.367	−1.443	−1.393	−1.392	<b>−1.454</b>
WSe <sub>2</sub>	<b>−1.606</b>	−1.469	−1.420	−1.419	−1.466

<sup>a</sup> The initial binding site of top-TM is unstable, and shift to a stable intermediate position (figure S1 of the supplementary material).

to be most favorable (table 1). In MoS<sub>2</sub>, top-TM is 48 meV more favorable than the next-most favorable site (bridge-B), and the difference between most and least favorable sites being 143 meV. MoSe<sub>2</sub> shows a smaller difference between binding site favorability, the difference between most and next-most favorable site being only 5 meV, with a difference between most and least favorable being 89 meV. This indicates high molecular mobility in MoSe<sub>2</sub>, as suggested experimentally in [31] for the case of MoS<sub>2</sub>, and is very similar to the energy differences between binding sites found amongst all TMDs in previous work [17]. WS<sub>2</sub> is mobile between the preferred top-Ch site and the next most favorable site of bridge-B, with a difference of only 12 meV. A difference of 87 meV separates the most and least favorable sites in WS<sub>2</sub>, implying good mobility across all sites, as in MoSe<sub>2</sub>. WSe<sub>2</sub> shows a difference of 137 meV between most and next-most favorable sites and 188 meV between most and least favorable sites. The PEN molecule lies flat in all systems, with minimal tilting and bending. Binding distances for the most favorable adsorption sites, determined by measuring separation between the chalcogenide top layer (that closest to the PEN molecule) of the substrate surface and the center of mass of the PEN molecule, were 3.30 Å, 3.42 Å, 3.32 Å and 3.48 Å for MoS<sub>2</sub>, MoSe<sub>2</sub>, WS<sub>2</sub> and WSe<sub>2</sub> respectively. These values are similar in magnitude and nature to those found previously in the lower concentration ( $7 \times 4$  supercell) systems, with larger binding distances in Se systems, notably in spite of the larger adsorption energy of the WSe<sub>2</sub> system in particular (table 1). This is again thought to be explained by the larger vdW radius of a selenium atom compared to a sulphur atom (1.90 Å and 1.73 Å, respectively [32]).

Additionally, the top-TM site of MoS<sub>2</sub> is not stable, and shifts under relaxation to between top-TM and hollow sites. This intermediate site between top-TM and hollow (figure S1 of the supplementary material) is, however, more favorable than the other sites investigated for this system. When rotating the PEN molecule on  $6 \times 3$  MoS<sub>2</sub>, both the shifted site and the ‘true’ top-TM site (where the shift towards hollow was not permitted) were investigated. The ‘true’ top-TM system was less favorable than the intermediate site when rotated and fully relaxed, and so was not investigated further. As the ‘true’ top-TM site is not entertained going forward, the intermediate binding site shall be referred to simply as top-TM, as the PEN was over this site prior to initial relaxation.

Adsorption energies ( $E_{\text{ads}}$ ) of PEN/TMD systems, displayed in table 1, were calculated as the difference between the combined system’s energy ( $E_{\text{PEN/TMD}}$ ) and the sum of the energies of the isolated systems with independently relaxed geometry ( $E_{\text{TMD}}^{\text{relax}}$  and  $E_{\text{PEN}}^{\text{iso-relax}}$ ) as in equation (1).

$$E_{\text{ads}} = E_{\text{PEN/TMD}} - E_{\text{TMD}}^{\text{relax}} - E_{\text{PEN}}^{\text{iso-relax}}. \quad (1)$$

A comparison of the structural properties between 0° PEN adsorbed on  $6 \times 3$  TMD and previous work on  $7 \times 4$  TMD [17] is provided in table 2.  $7 \times 4$  systems consistently preferred a top-Ch binding site, while there was variation within the  $6 \times 3$  systems. As discussed in this previous work, the most favorable binding

**Table 2.** Structural comparison of 0° pentacene adsorbed on TMDs for  $6 \times 3$  (higher molecular concentration) and  $7 \times 4$  (lower molecular concentration) supercells.  $7 \times 4$  parameters are from [17].

TMD	MoS <sub>2</sub>	MoSe <sub>2</sub>	WS <sub>2</sub>	WSe <sub>2</sub>
$6 \times 3$				
Binding site	Top-TM	Bridge-B	Top-Ch	Bridge-A
Adsorption energy (eV)	−1.46	−1.44	−1.45	−1.61
Binding distance (Å)	3.30	3.42	3.32	3.48
Minimum molecule–molecule distance (Å)	3.4	3.7	3.4	3.7
$7 \times 4$				
Binding site	Top-Ch	Top-Ch	Top-Ch	Top-Ch
Adsorption energy (eV)	−1.39	−1.42	−1.43	−1.46
Binding distance (Å)	3.31	3.40	3.30	3.38
Minimum molecule–molecule distance (Å)	6.2	6.5	6.2	6.5

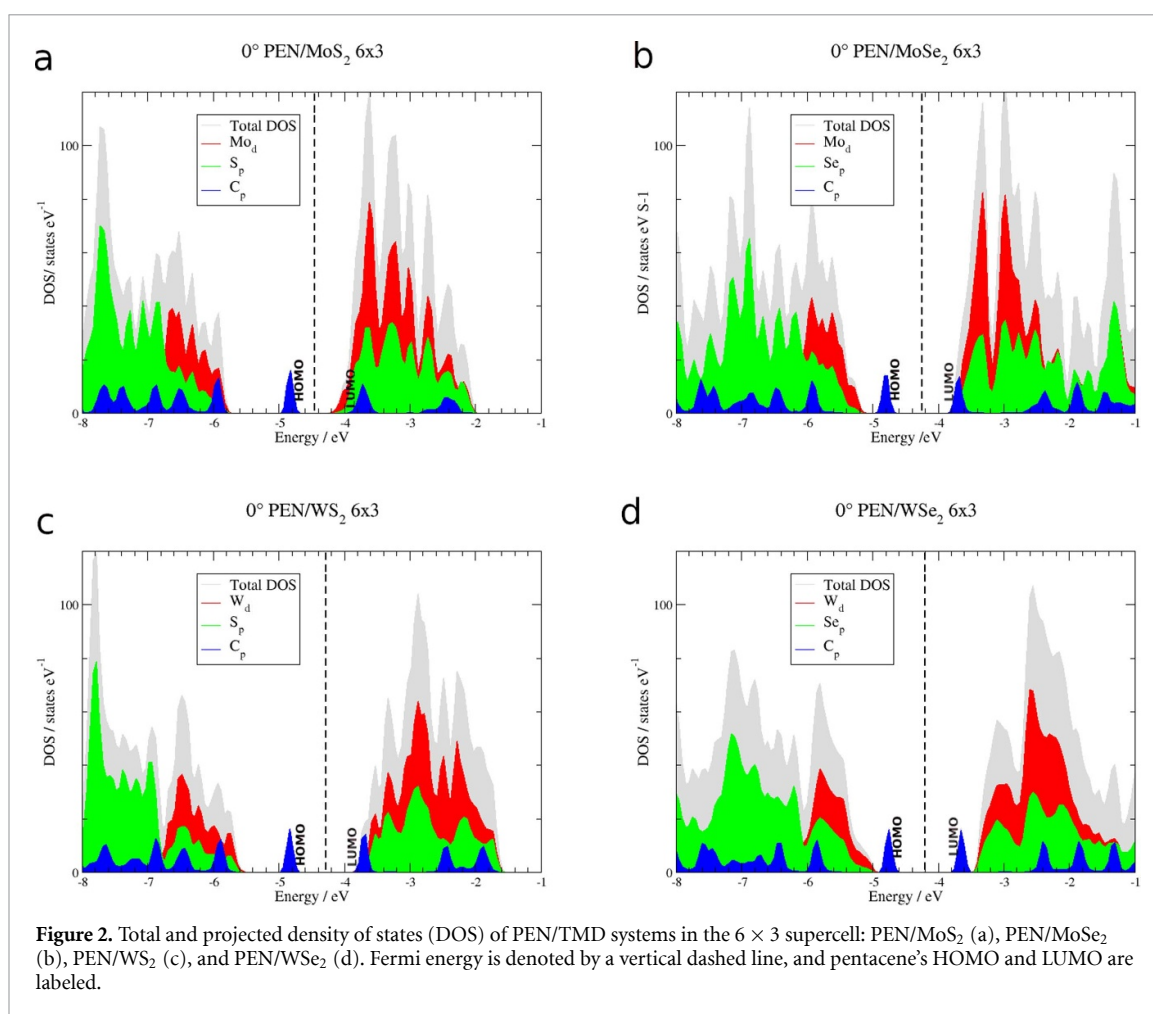
site in a  $7 \times 4$  system is that in which carbon atoms are not located over chalcogen atoms (transition metal atoms being less important due to their greater distance from the PEN atoms), reducing steric repulsion. For a  $6 \times 3$  system this is still generally true, but the additionally increased interaction with adjacent molecules reduces the relative importance in the context of favorable binding site. The  $7 \times 4$  systems demonstrated consistently lower differences in adsorption energy between binding sites, between 2 meV and 6 meV higher energy than the most favorable top-Ch site for the next-most favorable (bridge-B in all  $7 \times 4$  systems) site, and between 24 meV and 83 meV higher energy between the other sites [17]. In contrast, the  $6 \times 3$  systems demonstrate a much larger range of differences (between 5 meV and 188 meV), with overall larger energy differences between sites (the 5 meV being followed by the next smallest energy difference of 48 meV), implying a much more restricted molecular mobility between binding sites than found in the  $7 \times 4$  systems. Adsorption energies for favorable  $7 \times 4$  TMDs increased in magnitude with increasing substrate mass, with MoSe<sub>2</sub> and WS<sub>2</sub> being similar, and the  $6 \times 3$  systems did not follow this pattern. However; as they favor different binding sites, a direct comparison of adsorption energies is not expected to provide the same pattern.

Separation between PEN and TMD varied in the same manner for both concentrations (see table 2), with the sulphide systems showing binding at closer range, with the  $7 \times 4$  systems binding tighter than their  $6 \times 3$  counterparts, in particular for WSe<sub>2</sub>. A similar finding has been previously reported for PEN adsorbed on metal Ag(111) surface, where binding distances were found to increase with molecular concentration due to competing effects of molecule–molecule and molecule–substrate interactions [33]. These interactions are those between a PEN molecule and other PEN molecules across the imposed periodic boundary conditions, and those between a PEN molecule and the underlying substrate, respectively.

DOS was investigated for the most favorable binding sites of each TMD system in the  $6 \times 3$  supercell, in all cases demonstrating that PEN's highest occupied molecular orbital (HOMO), contributed by carbon p-orbitals, is located within the TMD band gap (figure 2). This state is closer to the TMD's valence band maximum (VBM) in the selenide systems than it is in the sulphide systems, explaining in part why there is stronger interaction between PEN and WSe<sub>2</sub> than in WS<sub>2</sub>. This difference in proximity is not as marked in the molybdenum systems, and so the same difference in adsorption energy is not seen between MoSe<sub>2</sub> and MoS<sub>2</sub>.

PEN's lowest unoccupied molecular orbital (LUMO) is located above the conduction band minimum (CBM) of sulphide systems (although this is a close distinction in WS<sub>2</sub>, see figures 2(a) and (c), indicating a staggered band gap, and so that these systems are type-II heterostructures. Selenide systems (figures 2(b) and (d)), however, show a type-I band alignment, with PEN's LUMO of lower energy than the TMD's CBM, with both of PEN's HOMO and LUMO within the TMD's band gap in the case of the selenide systems, seen as carbon p-orbital states in figures 2(b) and (d). In PEN/WS<sub>2</sub> (figure 2(c)), PEN's LUMO is very close to the TMD's CBM, but does display type-II alignment.

A comparison between the DOS of the two concentration regimes ( $6 \times 3$  and  $7 \times 4$  supercells [17]) is shown in figure S8 of the supplementary material. The DOS of the two concentration regimes are strikingly similar, both sets showing an inter-gap state contributed by the PEN's carbon p-orbital, closer to the TMD's VBM in selenide systems than in sulphide, and creating a type-II band alignment in sulphide systems in both concentrations investigated, type-I band alignment in WSe<sub>2</sub> structures in both concentrations, and a concentration dependency in PEN/MoSe<sub>2</sub>. The Fermi energies are similar, with PEN/MoS<sub>2</sub> decreasing from −4.42 eV to −4.45 eV with increased PEN concentration, PEN/MoSe<sub>2</sub> decreasing from −4.21 eV to −4.25 eV, and PEN/WSe<sub>2</sub> from −4.17 eV to −4.20 eV, but PEN/WS<sub>2</sub> increasing from −4.28 eV to −4.26 eV. The positions of PEN's HOMO and LUMO are also similar, with changes in LUMO energy due to increased PEN concentration of −0.08 eV (PEN/MoS<sub>2</sub>), −0.04 eV (PEN/MoSe<sub>2</sub>), −0.08 eV (PEN/WS<sub>2</sub>) and −0.09 eV



(PEN/WSe<sub>2</sub>). Despite having the smallest change in LUMO, PEN/MoSe<sub>2</sub> undergoes a band alignment transition due to the proximity of PEN's LUMO to the CBM in the  $7 \times 4$  supercell, with the small change in LUMO from increasing concentration being enough to cause the transition. The HOMO and LUMO positions of PEN/MoSe<sub>2</sub> in the  $7 \times 4$  system between  $0^\circ$  and  $60^\circ$  are undifferentiable within our precision, meaning that the observed changes are primarily due to the changes in concentration. Additionally, a comparison of the DOS of isolated PEN with PEN molecules in  $7 \times 4$  and  $6 \times 3$  supercells (but without the substrate) demonstrate a LUMO shift comparable to that found between the PEN/MoSe<sub>2</sub>  $7 \times 4$  and  $6 \times 4$  systems; the shift in PEN's LUMO responsible for the band alignment transition is due to molecule–molecule interaction. HOMO and LUMO energies of PEN in both higher ( $6 \times 3$ ) and lower ( $7 \times 4$ ) concentrations can be found in table S3 of the supplementary material, and the frontier orbital DOS of PEN at varying concentrations can be found in figure S3 of the supplementary material.

### 3.2. Effect of adsorbate rotation

The PEN molecule was then rotated about its center of mass in the plane of the two-dimensional substrate lattice (PEN remains flat-lying and maintains previously determined inter-layer separation) over the previously determined most favorable binding site for PEN/TMD systems. Rotation was with respect to the center of mass of PEN, with counterclockwise rotation angles of  $30^\circ$ ,  $60^\circ$  and  $90^\circ$  being investigated.  $0^\circ$  is defined as aligned with the long axis of the underlying substrate within the supercell. The rotated structures were then geometrically optimized, and the electronic properties of the resulting systems investigated.  $7 \times 4$  supercell systems were likewise rotated and compared, with starting geometry from [17]. The initial MoS<sub>2</sub> systems following the rotation of PEN, but before geometric optimization, are shown in figure 3; these are qualitatively representative of the other TMD systems.

#### 3.2.1. Higher molecular concentration: one PEN molecule per $6 \times 3$ supercell

As displayed in table 3, when rotating PEN in the high concentration regime for favorable binding sites, PEN/MoS<sub>2</sub> favored  $0^\circ$  PEN, as did MoSe<sub>2</sub>. The tungsten systems, however, were more energetically favorable after undergoing rotation: both WS<sub>2</sub> and WSe<sub>2</sub> favored a  $60^\circ$  rotation, which remains stable under



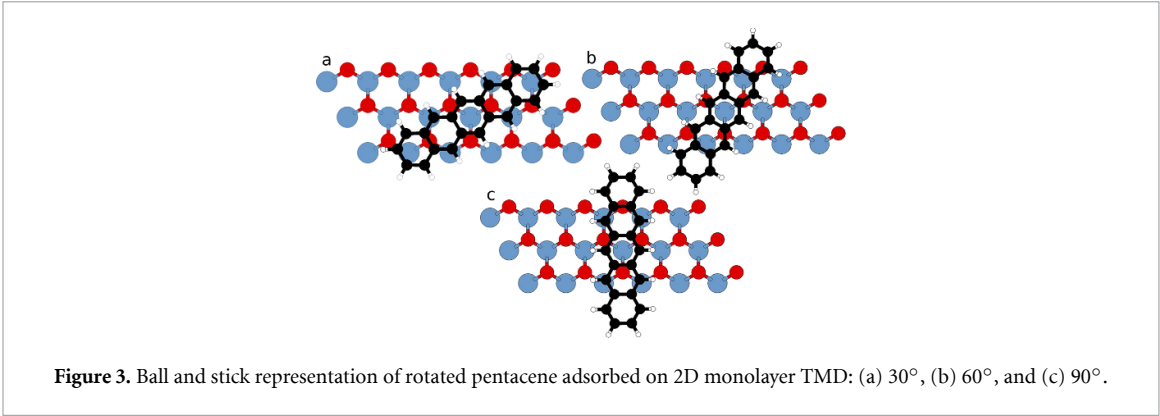


**Table 3.** Adsorption energies in eV following relaxation of rotated PEN/TMD systems in the  $6 \times 3$  supercell, starting from the most energetically favorable binding site (tables 1 and 2). The most favorable rotation angles for each heterostructure are displayed in bold.

TMD	0°	30°	60°	90° <sup>a</sup>
MoS <sub>2</sub>	<b>−1.461</b>	−1.371	−1.299	−1.302
MoSe <sub>2</sub>	<b>−1.437</b>	−1.385	−1.356	−1.405
WS <sub>2</sub>	−1.455	−1.427	<b>−1.461</b>	−1.413
WSe <sub>2</sub>	−1.606	−1.637	<b>−1.682</b>	−1.667

<sup>a</sup> 90° is the starting angle, but is unstable and shifts to 79° in MoS<sub>2</sub>, 70° in WS<sub>2</sub>, or 74° in selenide systems.

**Table 4.** Summary of the structural properties of PEN/TMD with  $6 \times 3$  supercells, considering rotation of the adsorbate.

TMD	Binding site	Rotation	Adsorption energy (eV)	Binding distance (Å)
MoS <sub>2</sub>	Top-TM	0°	−1.461	3.30
MoSe <sub>2</sub>	Bridge-B	0°	−1.437	3.42
WS <sub>2</sub>	Top-Ch	60°	−1.461	3.32
WSe <sub>2</sub>	Bridge-A	60°	−1.682	3.46

relaxation. None of the high PEN concentration systems remained stable under relaxation when starting at 90° rotated PEN; MoS<sub>2</sub> relaxed to an angle of 79°, WS<sub>2</sub> to 70°, and the selenide systems to 74°. 30° and 60° starting angles remained stable under relaxation in all systems. Minimum molecule–molecule separations of the favorable rotated systems were 3.1 Å and 3.4 Å for WS<sub>2</sub> and WSe<sub>2</sub> respectively. Table 4 summarizes the favorability of the rotated high concentration regime.

Unfavorable rotation angles for PEN/MoS<sub>2</sub> are between 90 meV and 160 meV less energetically favorable, implying a lack of mobility in angle of rotation, similar to the immobile binding sites in  $6 \times 3$  PEN/TMD systems, and in contrast to those in the  $7 \times 4$  systems, while PEN/MoSe<sub>2</sub> demonstrates higher energies of 32 meV to 81 meV for rotated systems. PEN/WS<sub>2</sub> has higher energies of 6 meV to 48 meV of the less favorable rotations than the most favorable 60°, but the least favorable investigated is the 70° rotation, and next-most favorable is the 0° system. WSe<sub>2</sub> demonstrates a difference between the most favorable 60° and next-most favorable 74° of only 15 meV, and a difference of 76 meV between most and least favorable rotations. This implies some mobility between the 60° and 74° rotations, with the starting angle of 90° to 74° or 79° supporting the concept in these systems, except for WS<sub>2</sub> (although the difference is only 48 meV, not much higher than MoSe<sub>2</sub>’s difference to its next most favorable rotation).

Minimum molecule–molecule separation is smaller in the rotated systems, but molecule–molecule interaction is not a significant enough contributor to adsorption energy to prevent the tungsten systems from being more favorable in a rotated geometry. Binding distances were 3.32 Å and 3.46 Å for WS<sub>2</sub> and WSe<sub>2</sub>, respectively (see table 4), demonstrating no change in distance in the WS<sub>2</sub> system compared to its 0° geometry, and only a small change in the WSe<sub>2</sub> system.

By calculating the adsorption energy using isolated systems with independently relaxed geometries, contributions from molecule–substrate and molecule–molecule interactions, as well as molecule and substrate deformation can be calculated as previously done in [17], and are summarized in table 5.

Contributions from molecule–molecule interactions account for lateral vdW interactions between the molecules in the neighboring supercells, while contributions from molecule (substrate) deformation account for the deformation of the PEN molecule (TMD substrate) due to the interaction with the TMD (PEN

**Table 5.** Contributions towards the adsorption energy of favorable rotated  $6 \times 3$  systems of PEN/TMD from molecule–molecule and molecule–substrate interactions, and molecule and substrate deformation, in eV. Angles of rotation are given in parenthesis. Details of these calculations can be found in the supplementary material.

TMD	MoS <sub>2</sub> (0°)	MoSe <sub>2</sub> (0°)	WS <sub>2</sub> (60°)	WSe <sub>2</sub> (60°)
molecule–molecule interaction	−0.0592	−0.0375	−0.0651	−0.0381
molecule–substrate interaction	−1.398	−1.400	−1.393	−1.422
molecule deformation	−0.0088	−0.0053	−0.0093	−0.0072
substrate deformation	0.0016	0.0025	0.0032	−0.2180

**Table 6.** Adsorption energies in eV following relaxation of rotated PEN/TMD systems in the  $7 \times 4$  supercells, starting from the most energetically favorable binding site (top-Ch in all cases [17]). The most favorable rotation angles for each heterostructure are displayed in bold.

TMD	0°	30°	60°	90°
MoS <sub>2</sub>	−1.389	−1.361	<b>−1.390</b>	−1.370
MoSe <sub>2</sub>	−1.424	−1.386	<b>−1.425</b>	−1.422
WS <sub>2</sub>	−1.434	−1.399	<b>−1.436</b>	−1.407
WSe <sub>2</sub>	−1.458	−1.768	<b>−1.813</b>	−1.802

molecule). The equations used for the calculations of these contributions are presented in the supplementary material.

The largest contribution to adsorption energy is due to the molecule–substrate interaction, with other contributions being orders of magnitude smaller. This would be expected as the PEN molecule does not deform during relaxation. Molecule–molecule interaction is one order of magnitude higher than that calculated for  $7 \times 4$  supercells in [17], which is a consequence of the smaller separation between the molecules across periodic boundary conditions.

A comparison of the DOS of 0° and favorable rotated systems shows no large deviation, with band alignment unchanged, comparable Fermi energies, and similar projected DOS topography, as shown in figure S5 of the supplementary material.

### 3.2.2. Lower molecular concentration: one PEN molecule per $7 \times 4$ supercell

In the low concentration PEN regime ( $7 \times 4$  supercell of TMD crystal) all systems were previously found to be most favorable with PEN at the top-Ch site [17]. All four systems were found to be more energetically favorable when rotated by 60° about the center of mass from the original 0° orientation (table 6), in contrast to the high concentration regime where there was variability between the TMDs (similar to binding site). All systems were stable about their starting angles, and remained flat-lying without significant bending or tilting. The use of a  $7 \times 4$  TMD crystal supercell yields a minimum molecule–molecule separation of approximately 6.2 Å for 0° sulphide systems, and 6.5 Å for 0° selenide systems. When rotated, the minimum separation decreases to approximately 5.2 Å (6.0 Å) for 30° rotation, 5.9 Å (6.3 Å) for 60° rotation, and 1.9 Å (2.5 Å) for 90° rotation on sulphide (selenide) systems. Similar to previous observation in the 0° systems, we notice only a small number of carbon atoms located over TMD atoms, with many over the hollow site, reducing steric repulsion in the heterostructure with rotated PEN. This is a trend noticed in both the sulphide and the selenide systems. Binding distances of these 60° systems are 3.31 Å, 3.40 Å, 3.30 Å, and 3.39 Å for MoS<sub>2</sub>, MoSe<sub>2</sub>, WS<sub>2</sub> and WSe<sub>2</sub>, respectively. These are exceptionally similar to the unrotated systems [17], following the same pattern of more closely bound for molybdenum compared to tungsten systems (as well as having lower adsorption energies), but greater binding distances for selenide compared to sulphide systems.

As can be seen in table 6, the difference in adsorption energies between the 60° rotations and other angles were between 1 meV and 30 meV for MoS<sub>2</sub>, 1 meV and 38 meV in MoSe<sub>2</sub>, and 2 meV and 38 meV in WS<sub>2</sub>. WSe<sub>2</sub> does not share these similar energy discrepancies, with a range between 11 meV and 355 meV. All TMDs except WSe<sub>2</sub> showed only a slight energetic preference for 60° over 0° PEN, with the least favorable rotation being 30°. WSe<sub>2</sub> instead showed a large energy difference between 0° and 60° PEN, with 30° rotation being comparably less favorable than with other TMDs, and 90° being the next-most favorable rotation after 60°. PEN adsorbed on TMDs, other than WSe<sub>2</sub>, may therefore be mobile within its z-axis rotational degree of freedom around the 0° angles, with reduced mobility as it approaches 30°, which is an unfavorable angle, creating a local minima of adsorption energy. Beyond this energy barrier lies a minima of lower energy than around 0° somewhere around 60°. WSe<sub>2</sub> exhibits different behavior, with a very unfavorable position in 0° becoming more favorable as rotation angle increases away from this point.

In the same manner as for the  $6 \times 3$  TMD supercell systems, the contributions to adsorption energy from molecule–molecule interaction, molecule–substrate interaction and deformation of the molecule and of the

**Table 7.** Contributions towards the adsorption energy of favorable  $7 \times 4$  systems following rotation of pentacene from molecule–molecule and molecule–substrate interactions, and molecule and substrate deformation, in eV. The most favorable angle of rotation for each TMD is given in parenthesis.

TMD	MoS <sub>2</sub> (60°)	MoSe <sub>2</sub> (60°)	WS <sub>2</sub> (60°)	WSe <sub>2</sub> (60°)
molecule–molecule interaction	−0.0048	−0.0034	−0.0048	−0.0035
molecule–substrate interaction	−1.393	−1.422	−1.439	−1.461
molecule deformation	−0.0067	−0.0100	−0.0064	−0.0094
substrate deformation	0.0060	0.0011	0.100 17	−0.3456

**Table 8.** Structural comparison of favorable systems of pentacene adsorbed on TMDs, considering rotation of the pentacene molecule.

TMD	MoS <sub>2</sub>	MoSe <sub>2</sub>	WS <sub>2</sub>	WSe <sub>2</sub>
$6 \times 3$				
Angle of rotation	0°	0°	60°	60°
Adsorption energy (eV)	−1.46	−1.44	−1.44	−1.68
Binding distance (Å)	3.30	3.42	3.32	3.46
Minimum molecule–molecule distance (Å)	3.4	3.7	3.1	3.4
$7 \times 4$				
Angle of rotation	60°	60°	60°	60°
Adsorption energy (eV)	−1.39	−1.42	−1.44	−1.81
Binding distance (Å)	3.31	3.40	3.30	3.39
Minimum molecule–molecule distance (Å)	5.9	6.3	5.9	6.3

substrate can be calculated and are displayed in table 7. Again it is found that molecule–substrate interaction is the largest contributor, but in the low concentration regime other sources are orders of magnitude smaller only in molybdenum systems. In both tungsten systems, substrate deformation is responsible for a relatively large amount of the adsorption energy, and in the case of WS<sub>2</sub>, *opposes* heterostructure formation. In the unrotated systems, this opposition is found in substrate deformation for all systems *except* WS<sub>2</sub>, but it is of much smaller magnitude [17]. As would be expected, the larger supercell (leading to greater separation of molecules when compared to the  $6 \times 3$  regime) results in a molecule–molecule interaction contribution much less significant than in the high concentration PEN regime. No significant difference was observed when compared to 0° rotation [17].

A comparison of the DOS of 0° heterostructures and favorable rotated systems again shows no marked change with unchanged band alignment, and comparable Fermi energies and projected DOS contributions (figure S7 of the supplementary material).

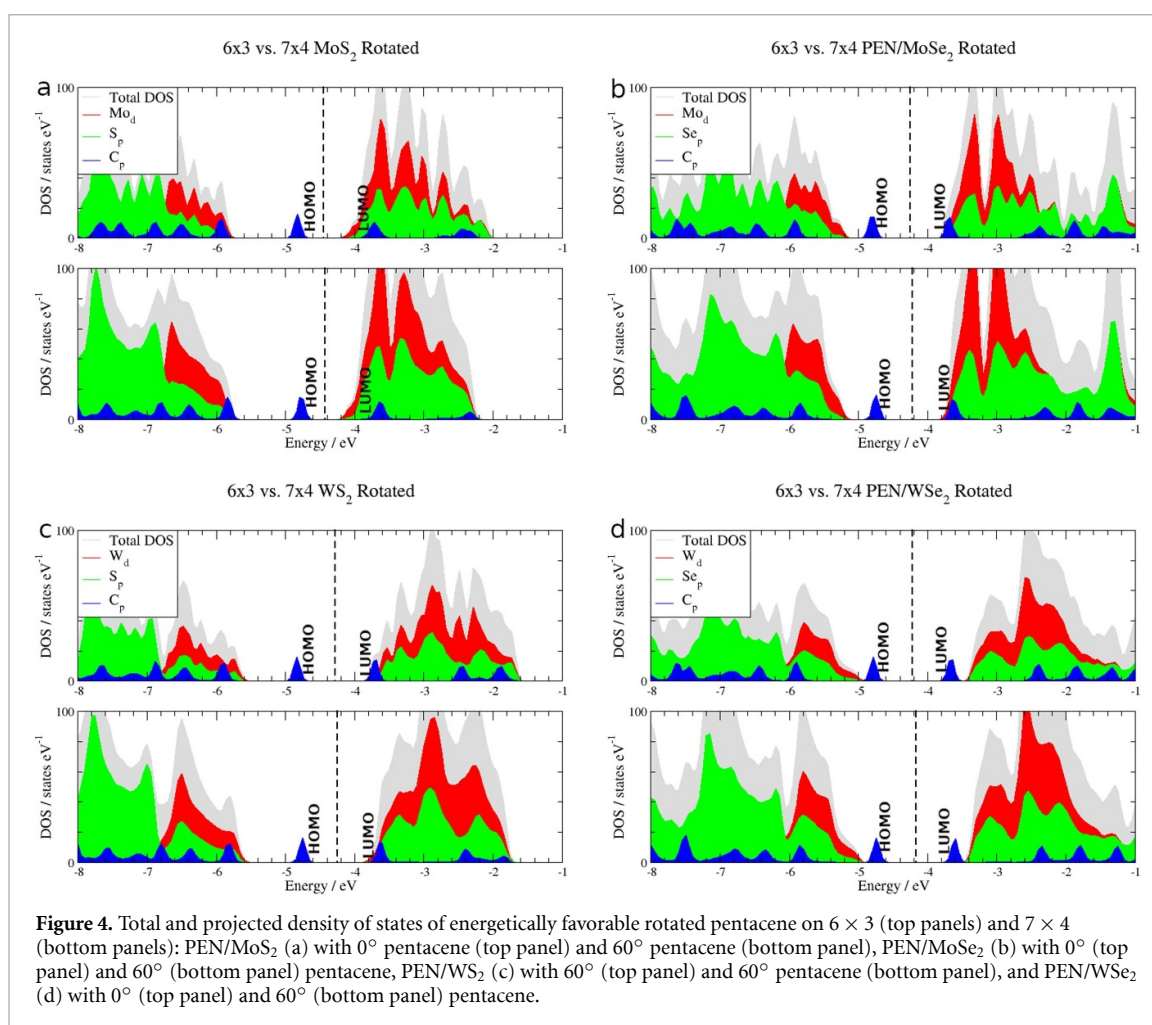
### 3.3. A comparison of favorably rotated systems

Table 8 is a comparison of structural properties between the favorable  $6 \times 3$  and  $7 \times 4$  TMD supercell systems, after rotation. The  $7 \times 4$  systems were consistent in their preferred binding site, while the  $6 \times 3$  systems were not. It is noted that most systems prefer 60° rotation, and it is the systems with lowest mass per supercell that does not prefer 60°; as the total substrate mass per supercell increases, and so does electron density ( $8.51 \text{ e}^- \text{ Å}^{-2}$ ,  $11.68 \text{ e}^- \text{ Å}^{-2}$ ,  $12.16 \text{ e}^- \text{ Å}^{-2}$  and  $15.13 \text{ e}^- \text{ Å}^{-2}$  for MoS<sub>2</sub>, MoSe<sub>2</sub>, WS<sub>2</sub> and WSe<sub>2</sub>, respectively, the same for both  $6 \times 3$  and  $7 \times 4$  systems). In the  $7 \times 4$  systems, and  $6 \times 3$  selenide systems, the preferred angle is 60°. The  $6 \times 3$  systems exhibit differences in adsorption energies between the most favorable and the next-most favorable rotations of between 90 meV, 32 meV, 6 meV and 15 meV for MoS<sub>2</sub>, MoSe<sub>2</sub>, WS<sub>2</sub> and WSe<sub>2</sub>, respectively. The  $7 \times 4$  systems instead are much more mobile in their PEN's z-axis rotational freedom, as previously discussed, with differences of 1 meV for both molybdenum systems, 2 meV for WS<sub>2</sub>, and a slightly larger 11 meV for WSe<sub>2</sub>.

Binding distances followed the pattern shown by 0° systems, with very similar separation between layers compared to both concentration regime's unrotated counterparts. The  $6 \times 3$  tungsten systems, that preferred an angle other than 0°, adsorb at a greater distance from the substrate than the  $7 \times 4$  tungsten systems, but the molybdenum systems are similar between concentration regimes.

DOS calculations (the results of which are displayed in figure 4) show no changes to the character of the heterojunctions upon decreasing molecular concentration on MoS<sub>2</sub>, WS<sub>2</sub> or WSe<sub>2</sub> substrates, with PEN/WSe<sub>2</sub> remaining a type-I heterojunction and the other sulphide systems exhibiting type-II band alignment. The PEN/MoSe<sub>2</sub> heterojunction, however, undergoes a transition from a type-II (staggered) band alignment in the lower concentration regime ( $7 \times 4$  supercell) to a type-I (straddled) band alignment with increased molecular concentration ( $6 \times 3$  supercell). All systems maintain their intergap state contributed by





PEN's carbon p-orbital and the Fermi energies are negligibly changed, although it is noted that changing the concentration of PEN has a larger effect on the Fermi energy than rotating the adsorbate alone.

## 4. Conclusions

In summary, adsorbed PEN of two different concentrations and four angles of rotation with respect to the substrate's long axis have been investigated on the 2D monolayer TMD substrates of MoS<sub>2</sub>, MoSe<sub>2</sub>, WS<sub>2</sub> and WSe<sub>2</sub>. PEN lies flat in all systems, and binds more strongly when in the lower concentration. High concentration PEN yields variation in favorable adsorption site and angle of rotation between the investigated TMDs, with mobility between adsorption sites being generally reduced when compared to the lower concentration regime, whereas low concentration PEN adsorbs most favorably in the same site and at the same angle across all investigated TMDs. Band alignment of the PEN/TMD heterostructures is robust to changes in the angle of PEN and the change in concentration investigated here (but band tuning was observed), with the exception of MoSe<sub>2</sub>. PEN/MoSe<sub>2</sub> undergoes a band alignment transition between the low and high PEN concentration regimes, from a type-II to a type-I.

## Data availability statement

The data that support the findings of this study are openly available at Keele Data Repository: <https://doi.org/10.21252/dbmt-tf28>.

## Acknowledgments

This work was partially funded by the Deutsche Forschungsgemeinschaft (DFG, German Research Foundation), Project 406901005. Calculations were performed using the Cirrus UK National Tier-2 HPC Service at EPCC ([www.cirrus.ac.uk](http://www.cirrus.ac.uk)) funded by the University of Edinburgh and EPSRC (EP/P020267/1).

## ORCID iDs

E Black  <https://orcid.org/0009-0008-5956-3533>

J M Morbec  <https://orcid.org/0000-0002-1672-3575>

## References

- [1] Dong R and Kuljanishvili I 2017 Progress in fabrication of transition metal dichalcogenides heterostructure systems *J. Vac. Sci. Technol. B* **35** 030803
- [2] Liu Y, Weiss N O, Duan X, Cheng H-C, Huang Y and Duan X 2016 Van der Waals heterostructures and devices *Nat. Rev. Mater.* **1** 1–17
- [3] Geim A K and Grigorieva I V 2013 Van der Waals heterostructures *Nature* **499** 419–25
- [4] Zhao W, Ribeiro R M and Eda G 2015 Electronic structure and optical signatures of semiconducting transition metal dichalcogenide nanosheets *Acc. Chem. Res.* **48** 91–99
- [5] Li Q, Lu J, Gupta P and Qiu M 2019 Engineering optical absorption in graphene and other 2D materials: advances and applications *Adv. Opt. Mater.* **7** 1900595
- [6] Kumar R, Verzhbitskiy I and Eda G 2015 Strong optical absorption and photocarrier relaxation in 2-D semiconductors *IEEE J. Quantum Electron.* **51** 1–6
- [7] Wong J, Jariwala D, Tagliabue G, Tat K, Davoyan A R, Sherrott M C and Atwater H A 2017 High photovoltaic quantum efficiency in ultrathin van der Waals heterostructures *ACS Nano* **11** 7230–40
- [8] Wi S, Kim H, Chen M, Nam H, Guo L J, Meyhofer E and Liang X 2014 Enhancement of photovoltaic response in multilayer MoS<sub>2</sub> induced by plasma doping *ACS Nano* **8** 5270–81
- [9] Liu W, Kang J, Sarkar D, Khatami Y, Jena D and Banerjee K 2013 Role of metal contacts in designing high-performance monolayer n-type WSe<sub>2</sub> field effect transistors *Nano Lett.* **13** 1983–90
- [10] Withers F *et al* 2015 Light-emitting diodes by band-structure engineering in van der Waals heterostructures *Nat. Mater.* **14** 301–6
- [11] Singh E, Singh P, Kim K S, Yeom G Y and Nalwa H S 2019 Flexible molybdenum disulfide (MoS<sub>2</sub>) atomic layers for wearable electronics and optoelectronics *ACS Appl. Mater. Interfaces* **11** 11061–105
- [12] Li B L, Luo H Q, Lei J L and Li N B 2014 Hemin-functionalized MoS<sub>2</sub> nanosheets: enhanced peroxidase-like catalytic activity with a steady state in aqueous solution *RSC Adv.* **4** 24256–62
- [13] Wang J *et al* 2018 Charge transfer within the F<sub>4</sub>TCNQ-MoS<sub>2</sub> van der Waals interface: toward electrical properties tuning and gas sensing application *Adv. Funct. Mater.* **28** 1806244
- [14] Maliakal A, Raghavachari K, Katz H, Chandross E and Siegrist T 2004 Photochemical stability of pentacene and a substituted pentacene in solution and in thin films *Chem. Mater.* **16** 4980–6
- [15] Nelson S, Lin Y-Y, Gundlach D and Jackson T N 1998 Temperature-independent transport in high-mobility pentacene transistors *Appl. Phys. Lett.* **72** 1854–6
- [16] Kim S, Choi Y, Kim K, Kim J and Im S 2003 Fabrication of p-pentacene/n-Si organic photodiodes and characterization of their photoelectric properties *Appl. Phys. Lett.* **82** 639–41
- [17] Black E, Kratzer P and Morbec J 2023 Interaction between pentacene molecules and monolayer transition metal dichalcogenides (arXiv:2304.08619)
- [18] Bettis Homan S, Sangwan V K, Balla I, Bergeron H, Weiss E A and Hersam M C 2017 Ultrafast exciton dissociation and long-lived charge separation in a photovoltaic pentacene–MoS<sub>2</sub> van der Waals heterojunction *Nano Lett.* **17** 164–9
- [19] Habib M R, Wang W, Khan A, Khan Y, Obaidulla S M, Pi X and Xu M 2020 Theoretical study of interfacial and electronic properties of transition metal dichalcogenides and organic molecules based van der Waals heterostructures *Adv. Theory Simul.* **3** 2000045
- [20] Markeev P A *et al* 2022 Exciton dynamics in MoS<sub>2</sub>-pentacene and WSe<sub>2</sub>-pentacene heterojunctions *ACS Nano* **16** 16668–76
- [21] Mete E, Demiroglu İ, Fatih Danisman M and Ellialtıoglu Ş 2010 Pentacene multilayers on Ag(111) surface *J. Phys. Chem. C* **114** 2724–9
- [22] Satta M, Iacobucci S and Larciprete R 2007 Molecular adsorption and multilayer growth of pentacene on Cu(100): layer structure and energetics *Phys. Rev. B* **75** 155401
- [23] Sun X, Suzuki T, Yamauchi Y, Kurahashi M, Wang Z and Entani S 2008 Ab initio study of pentacene on the Fe(100) surface *Surf. Sci.* **602** 1191–8
- [24] Kohn W and Sham L J 1965 Self-consistent equations including exchange and correlation effects *Phys. Rev.* **140** A1133
- [25] Giannozzi P *et al* 2009 QUANTUM ESPRESSO: a modular and open-source software project for quantum simulations of materials *J. Phys.: Condens. Matter* **21** 395502
- [26] Giannozzi P *et al* 2017 Advanced capabilities for materials modelling with QUANTUM ESPRESSO *J. Phys.: Condens. Matter* **29** 465901
- [27] Perdew J P, Burke K and Ernzerhof M 1996 Generalized gradient approximation made simple *Phys. Rev. Lett.* **77** 3865
- [28] Grimme S, Antony J, Ehrlich S and Krieg H 2010 A consistent and accurate *ab initio* parametrization of density functional dispersion correction (DFT-D) for the 94 elements H–Pu *J. Chem. Phys.* **132** 154104
- [29] Blöchl P E 1994 Projector augmented-wave method *Phys. Rev. B* **50** 17953
- [30] Monkhorst H J and Pack J D 1976 Special points for brillouin-zone integrations *Phys. Rev. B* **13** 5188
- [31] Kachel S R, Dombrowski P-M, Breuer T, Gottfried J M and Witte G 2021 Engineering of TMDC–OSC hybrid interfaces: the thermodynamics of unitary and mixed acene monolayers on MoS<sub>2</sub> *Chem. Sci.* **12** 2575–85
- [32] Batsanov S S 2001 Van der Waals radii of elements *Inorg. Mater.* **37** 871–85
- [33] Duhm S *et al* 2013 Pentacene on Ag(111): correlation of bonding distance with intermolecular interaction and order *ACS Appl. Mater. Interfaces* **5** 9377–81